npj | precision oncology

Article

Published in partnership with The Hormel Institute, University of Minnesota

https://doi.org/10.1038/s41698-024-00682-y

Amivantamab efficacy in wild-type EGFR NSCLC tumors correlates with levels of ligand expression

Ricardo Rivera-Soto[1] ✉, Benjamin Henley[1], Marian A. Pulgar[1], Stacey L. Lehman[1], Himanshu Gupta[1], Kia Z. Perez-Vale[1], Megan Weindorfer[1], Smruthi Vijayaraghavan[1], Tsun-Wen Sheena Yao[2], Sylvie Laquerre[1] & Sheri L. Moores[1]

Amivantamab is an FDA-approved bispecific antibody targeting EGF and Met receptors, with clinical activity against EGFR mutant non-small cell lung cancer (NSCLC). Amivantamab efficacy has been demonstrated to be linked to three mechanisms of action (MOA): immune cell-mediated killing, receptor internalization and degradation, and inhibition of ligand binding to both EGFR and Met receptors. Among the EGFR ligands, we demonstrated that amphiregulin (AREG) is highly expressed in wild-type (WT) EGFR ($EGFR^{WT}$) NSCLC primary tumors, with significantly higher circulating protein levels in NSCLC patients than in healthy volunteers. Treatment of AREG-stimulated $EGFR^{WT}$ cells/tumors with amivantamab or with an AREG-targeting antibody inhibited ligand-induced signaling and cell/tumor proliferation/growth. Across 11 $EGFR^{WT}$ NSCLC patient-derived xenograft models, amivantamab efficacy correlated with *AREG* RNA levels. Interestingly, in these models, amivantamab anti-tumor activity was independent of Fc engagement with immune cells, suggesting that, in this context, the ligand-blocking function is sufficient for amivantamab maximal efficacy. Finally, we demonstrated that in lung adenocarcinoma patients, high expression of *AREG* and EGFR mutations were mutually exclusive. In conclusion, these data 1) highlight EGFR ligand AREG as a driver of tumor growth in some $EGFR^{WT}$ NSCLC models, 2) illustrate the preclinical efficacy of amivantamab in ligand-driven $EGFR^{WT}$ NSCLC, and 3) identify AREG as a potential predictive biomarker for amivantamab activity in $EGFR^{WT}$ NSCLC.

Over the past few decades, significant progress has been made toward understanding the biology and clinical management of non-small cell lung cancer (NSCLC). Driver mutations within receptor tyrosine kinases (RTK) have been identified, and inhibitors against these have been developed and approved, including drugs against mutant epidermal growth factor receptor (EGFR), which is altered in 10–40% of lung cancer patients[1]. Unfortunately, although patients initially respond to EGFR tyrosine kinase inhibitors (TKI), such as gefitinib or osimertinib, resistance inevitably emerges through additional EGFR mutations (e.g., T790M, C797S) or up-regulation of other driver pathways, such as Met. While inhibitors have been developed against mutant EGFR, few options are available for wild-type EGFR ($EGFR^{WT}$) NSCLC. $EGFR^{WT}$ can be activated by any of several EGFR ligands, which include amphiregulin (AREG), betacellulin (BTC), epidermal growth factor (EGF), epigen (EPGN), epiregulin (EREG), heparin-binding EGF (HB-EGF), or transforming growth factor alpha (TGFα). The binding of a ligand to the receptors induces a conformational change, resulting in the activation of the downstream signaling pathways[2,3].

To address the unmet need in patients who have failed multiple generations of EGFR TKI and to circumvent these mechanisms of resistance, we developed amivantamab (JNJ-61186372), a fully human IgG1-based bispecific antibody designed to target the EGF and Met RTKs[4,5]. Following the positive CHRYSALIS study results, amivantamab received initial regulatory approval for the treatment of patients with locally advanced or metastatic NSCLC with EGFR exon 20 insertion mutations whose disease has progressed on or after platinum-based chemotherapy in 2021[6]. Furthermore, recently published data from phase III trials show that the combination of amivantamab plus chemotherapy (PAPILLON trial) and the triple combination of amivantamab, chemotherapy, and lazertinib (MARIPOSA and

[1]Janssen Research and Development, Spring House, PA, USA. [2]Janssen Research and Development, La Jolla, CA, USA. ✉e-mail: rriver63@its.jnj.com

The Hormel Institute University of Minnesota

MARIPOSA 2 trials) was superior to the current standard of care[7–9]. The data from PAPILLON led to an additional FDA approval for the combination of amivantamab plus chemotherapy as a 1st line in EGFR exon 20 insertion-mutated NSCLC. Additional ongoing trials evaluate amivantamab in several indications, including esophageal and colorectal cancers.

Preclinical studies demonstrated that amivantamab inhibits mutant EGFR NSCLC growth with 3 potential mechanisms of action (MOA): 1) Fc-dependent interaction with immune cells to induce antibody-dependent cell cytotoxicity, antibody-dependent cell phagocytosis, and antibody-dependent cell trogocytosis; 2) blocking the interaction of the EGF and Met receptors with their ligands; and 3) antibody-induced internalization of the receptors in an Fc-independent manner[4,10,11].

We previously reported that amivantamab inhibits tumor growth in a variety of cell line-derived xenografts (CDX) and patient-derived xenograft (PDX) models, including those with wild-type or with activating mutations in the EGF and Met receptors[4,10]. Because ligands can induce the activation of the receptors independent of mutational status and previous reports suggest that expression levels of some EGFR ligands are associated with response to anti-EGFR therapies, we explored the role of ligands in EGFR^{WT} NSCLC preclinical models[12–14]. We demonstrate here that AREG is highly expressed in NSCLC tumors, and the circulating protein levels are significantly higher in NSCLC patients than in healthy volunteers. Furthermore, through in vitro and in vivo studies, we identified AREG as a driver of NSCLC tumor growth. Importantly, we found that across 11 EGFR^{WT} NSCLC PDX tumor models, amivantamab anti-tumor activity correlated with the mRNA levels of *AREG*. Lastly, analysis of data from The Cancer Genome Atlas suggested that in lung adenocarcinoma (LUAD) patients, high expression of AREG is statistically more frequently associated with patients lacking EGFR mutations. Finally, this study supports the ongoing clinical assessment of amivantamab as a therapeutic treatment for EGFR^{WT} disease and highlights AREG as a potential patient-selection biomarker.

Results

The EGFR ligand AREG is highly expressed in tumors and blood from NSCLC patients

Previously, we demonstrated that amivantamab was effective in reducing the tumor growth of an NSCLC cell line-derived xenograft lacking EGFR or Met activating mutations or amplifications[4]. This observation suggested that even in tumors lacking activating mutations in EGFR and Met, these receptors might play an essential role in tumor growth and survival. In the absence of activating mutations or gene amplifications, ligands contribute to the activation of the EGF and Met receptors and uncontrolled cancer cell growth. In the context of lung cancers, the Met receptor ligand, hepatocyte growth factor (HGF), is produced by mesenchymal cells and fibroblasts, and murine HGF does not bind or activate human Met on human tumor xenografts. Therefore, we initially focused on the EGFR ligands as factors that may contribute to NSCLC tumor growth in the absence of common driver mutations[2,15,16].

To assess the expression of various EGFR ligands in tumor samples from EGFR^{WT} NSCLC patients, we performed ELISA to evaluate the protein levels of the EGFR ligands AREG, BTC, EGF, EREG, HB-EGF, and TGFα from 15 tumors. The expression of these EGFR ligands was measured, with AREG showing the highest level of expression (Fig. 1A). In addition, the expression of circulating levels of 6 of these EGFR ligands (AREG, BTC, HB-EGF, EGF, EREG, and TGFα) was assessed in the peripheral blood of healthy and NSCLC donors. The results showed that the levels of AREG and HB-EGF were significantly higher in patients than in healthy volunteers, while the other ligands tested showed similar levels in healthy and diseased samples (**$P < 0.01$; Fig. 1B and Supplementary Fig. 1). Although BTC was measured in serum samples, the data was not included because no samples were above the lower limit of quantification. Thus, these data demonstrate that AREG is highly expressed in tumors and blood obtained from EGFR^{WT} NSCLC patients.

AREG induces EGFR signaling and proliferation of NSCLC cell lines

Previous reports suggested a link between AREG expression and clinical response to EGFR inhibition[12–14,17], so we further explored the role of AREG on the proliferation and tumor growth of NSCLC cells and the effect of amivantamab in the context of ligand-induced proliferation. We confirmed the ability of AREG to induce EGFR dimerization, the initial step leading to receptor activation[2]. In this assay, the Enzyme Fragment Complementation technology, where β-galactosidase (β-gal) activity requires dimerization of its spitted two fragments fused to EGFR monomers, was used in engineered U2OS cells. Upon dimerization of EGFR, active β-gal cleaves its substrate leading to a quantifiable chemiluminescent signal. Recombinant AREG (rAREG) induces EGFR dimerization in a dose-dependent manner with an EC50 of 77 ng/mL (Supplementary Fig. 2Ai). Using this assay, we demonstrated that amivantamab, but not an isotype control, reduces AREG-induced EGFR dimerization in a dose-dependent manner (Supplementary Fig. 2Aii).

The capability of AREG to stimulate the activation of EGFR in NSCLC cells was assessed by western blots and AlphaLISA upon treatment of serum-starved H292 cells (EGFR^{WT}) with 100–1000 ng/mL of rAREG in absence or presence of either amivantamab or low-fucose isotype control (Isotype; Fig. 2A and Supplementary Fig. 2B, C). A strong induction of phosphorylation of multiple EGFR residues (Y1173, T669, Y1086) and downstream effectors such as Erk and Akt was seen in the presence of AREG as early as 5 min post-stimulation. Moreover, the basal and AREG-induced phosphorylation of EGFR and its downstream signaling proteins were reduced in the presence of amivantamab but not with the isotype control antibody. Furthermore, through AlphaLISAs we confirmed that amivantamab reduces AREG-induced phosphorylation in a dose-dependent manner. These results confirm that rAREG induces phosphorylation of EGFR in H292 cells and that amivantamab efficiently blocks AREG-induced activation of EGFR signaling.

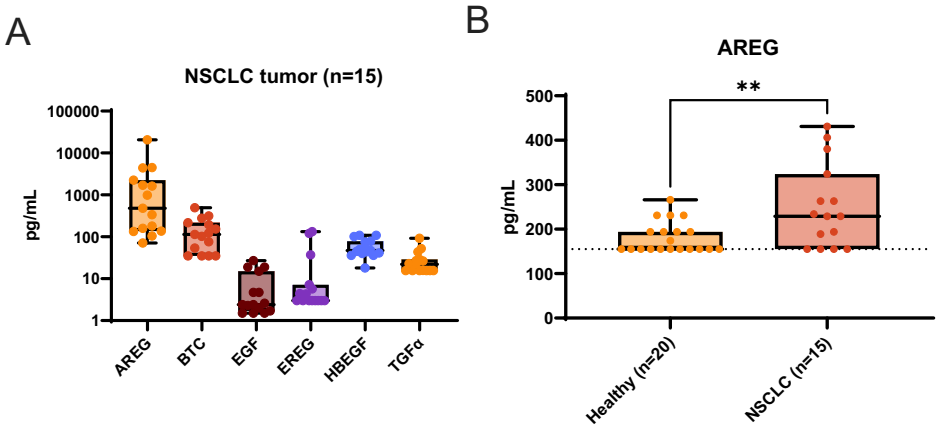

Fig. 1 | EGFR ligand levels in tumors and blood from NSCLC patients. A Fresh frozen tumor tissues collected on dry ice were homogenized into protein lysates. EGFR ligand levels were measured using protein-based assays. AREG, EGF, EREG, HB-EGF ligands were measured by HCANCER2 panel, BTC level by HMPC18 panel, and TGFα levels using ELISA. **B** Serum AREG levels of NSCLC patients and healthy volunteers were measured by Luminex-based assay. Samples below the assay detection range are plotted at the lower limit of quantification (dotted line). *P*-value was determined by Tobit regression analysis, **$P < 0.01$. Box-and-whisker plots represents min-to-max distribution with center lines at the median.

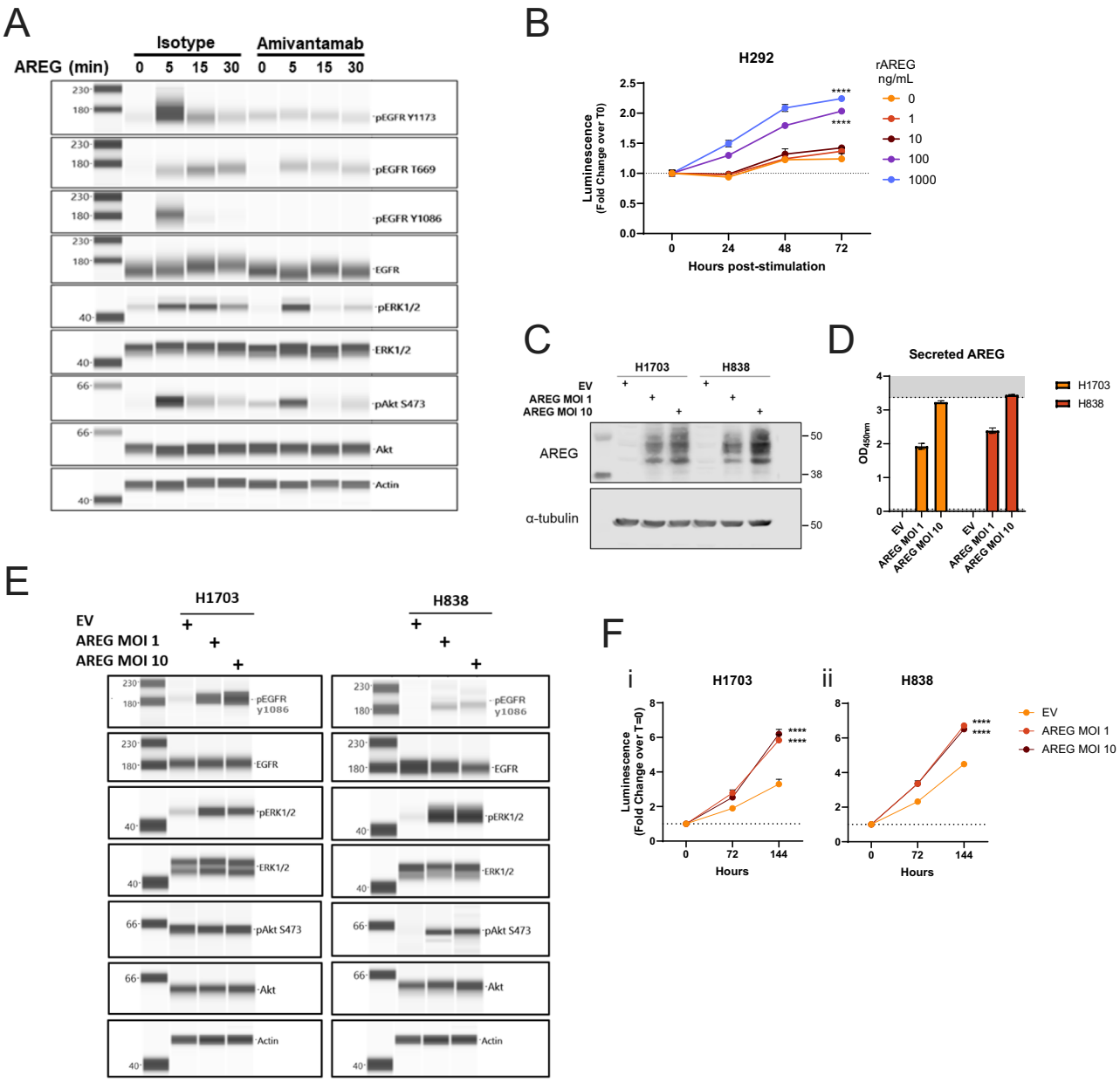

Fig. 2 | AREG induces signaling and proliferation of NSCLC cell lines. A NSCLC H292 cells were stimulated with 100 ng/mL of rAREG in the presence of 10 µg/mL of amivantamab or IgG1 isotype control (Isotype). Cells were harvested and lysed before stimulation (time 0) and at 5-, 15-, and 30 min post AREG treatment. Lysates were subjected to capillary-based electrophoresis to quantitate the levels of $pEGFR^{Y1173/T669/Y1086}$, EGFR, $pErk1/2^{T202/Y204}$, Erk1/2, $pAkt^{S473}$, Akt, and actin (as loading control). *Densitometry calculations are included in the* Supplementary Fig. 2B. **B** Serum-starved H292 cells were stimulated with increasing concentrations of rAREG. Luminescence compared to T0, determined by ATP-dependent CellTiter-Glo (CTG) assay, were plotted over a time-course (24, 48, and 72 h post-stimulation). Dotted line represents T0. *P*-value was determined by two-way ANOVA with Dunnet's multiple comparison tests; **** $P < 0.0001$. **C** AREG-low H1703 and H838 NSCLC cell lines were transduced at multiplicity of infection (MOI) of 1 or 10 with an AREG-containing lentiviruses or an empty vector control (EV). Equal amount of whole cell protein lysates was subjected to western blotting for AREG and loading control α-tubulin. *The densitometry calculations are included in the* Supplementary Fig. 2G. **D** Cell-free supernatants from H1703 and H838 cells stably expressing AREG were collected and AREG secretion measured by ELISA. *Gray areas = above/below the limit of detection*. **E** Stably expressing AREG H1703 and H838 cells were cultured overnight in low-serum conditions (1%) and whole cell lysates were collected and subjected to capillary-based electrophoresis for $pEGFR^{Y1086}$, EGFR, $pErk1/2^{T202/4}$, Erk1/2, $pAkt^{S473}$, Akt, and β-actin detection and quantification. *The densitometry calculations are included in the* Supplementary Fig. 2G. **F** H1703 **(i)** and H838 **(ii)** cells were cultured for up to 6 days (144 h) in low serum (1%) and cell number measured by CTG to determine cell proliferation over time (0, 72, and 144 h). Dotted line represents T0. *P*-value was determined by two-way ANOVAs with Dunnet's multiple comparison tests, ****$P < 0.0001$.

Similarly, we assessed the capability of the other 6 known EGFR ligands (BTC, EGF, EPGN, EREG, HB-EGF, TGFα) to activate EGFR and the inhibitory effect of amivantamab. H292 cells were incubated with EGFR ligands for 15 min in the presence of amivantamab and its isotype control. Except for EPGN, all tested ligands induced phosphorylation of EGFR, which is attenuated in the presence of amivantamab but not its isotype control antibody (Supplementary Fig. 2D). These results are in agreement with our previous report showing that amivantamab has a broad potential to block ligand-induced activation of EGFR[4].

As the phosphorylation of EGFR and the activation of downstream signaling might contribute to cell growth, we assessed whether AREG could stimulate $EGFR^{WT}$ NSCLC cell proliferation. H292 cells were cultured in

low-serum conditions for up to 3 days in presence or absence of rAREG, and cell growth was tracked using the ATP-dependent assay, CellTiter-Glo, over time. In this experiment, adding rAREG resulted in a dose-dependent increase in cell proliferation (Fig. 2B).

As the initial studies utilized rAREG, we next evaluated the contribution of endogenously expressed AREG by transfecting cell lines expressing low levels of AREG (H1703 and H838; Supplementary Fig. 2E) with empty vector (EV) or AREG-expressing lentivirus to generate AREG overexpressing (OE) cells. An increased AREG protein expression was confirmed by western blot from a pool of stable cells, and AREG secretion was evaluated using ELISA on cell-free supernatant (Fig. 2C and Supplementary Fig. 2F). As expected, cells transduced with the EV secreted minimal AREG. In contrast, cells transduced with the AREG-containing construct secreted high levels of AREG, confirming that AREG is efficiently trafficked and secreted from these OE cells (Fig. 2D). AREG functionality was assessed through quantification of pathway activation, including phosphorylation of EGFR and its downstream signaling pathway. In contrast to the cells transduced with EV, expression of AREG from AREG OE H1703 and H838 in serum-starved conditions increased pEGFR, pErk, pAkt, pP90RSK, pCREB, and pPS6K, suggesting that AREG is functional and active in these cells (Fig. 2E and Supplementary Fig. 2G, H). To assess the ability of endogenously expressed AREG to promote cell proliferation, AREG OE cells and the respective EV-transduced cell controls were cultured in low-serum conditions for up to 6 days. Similar to the effect seen with rAREG on H292 cells, overexpression of AREG significantly increased the proliferation of H1703 and H838 cells (Fig. 2F). Taken together, these results demonstrated that AREG induces EGFR signaling and promotes $EGFR^{WT}$ NSCLC cell proliferation.

AREG-neutralizing antibody blocks AREG-induced signaling and cell growth

To further confirm AREG's role in driving NSCLC cell proliferation, we assessed the ability of AREG-targeting antibodies to neutralize ligand-induced signaling and cell growth. Two previously described AREG-targeting antibody clones, AREGB1 (AR558) and AREGB2 (AR37), with minimal cross-reactivity to the other EGFR ligands[18], were produced in CHO cells. Capillary-based electrophoresis confirmed that both AREGB1 and AREGB2 efficiently blocked human (h)AREG-induced pEGFR in H292 cells (Fig. 3A and Supplementary Fig. 3A). Interestingly, AREGB2 showed improved blocking of downstream signaling capabilities compared to that of AREGB1, as determined by Erk phosphorylation. Previous studies demonstrated that besides targeting hAREG, AREGB2, but not AREGB1, also targets mouse (m)AREG[18]. To confirm this report, H292 cells were treated with 100 or 500 ng/mL of mAREG in the presence of AREGB1, AREGB2, or an IgG1 isotype control. Results confirmed the previous publication, showing that AREGB2 substantially blocked mAREG-induced pEGFR (Fig. 3B and Supplementary Fig. 3B). Further, the ability of AREGB2 and amivantamab to block both human and mouse rAREG-induced pEGFR and pErk was confirmed by AlphaLISA (Supplementary Fig. 3C). To assess the anti-proliferative activity of AREGB2 on ligand-induced cell proliferation, H292 cells were stimulated with rAREG in the presence of AREGB2, amivantamab, or an isotype control antibody. Treatment with either amivantamab or AREGB2 resulted in a dose-dependent decrease of H292 cell proliferation (Fig. 3C and Supplementary Fig. 3D). Furthermore, treatment with the EGFR monovalent antibody (EGFR-binding arm of amivantamab and a nonbinding arm (EGFRxRSV)) reduced the proliferation of AREG-stimulated H292 cells (Supplementary Fig. 3E). In contrast, treatment with the Met monovalent antibody (one Met-binding arm of amivantamab and a nonbinding arm (Met x RSV)) showed no inhibitory effect on the AREG-induced proliferation of H292 cells. These results demonstrated that amivantamab and AREGB2 inhibition in H292 cell proliferation is mediated by blockade of EGFR signaling.

As the H292 cells may intrinsically depend on AREG-induced signaling, sensitivity to AREG or EGFR inhibition was also assessed on AREG-OE H1703 and H838 cells. For both cell lines, as expected, treatment of EV-transduced cells with amivantamab or AREGB2 did not affect cell proliferation. However, treatment of AREG-OE cells with AREGB2, amivantamab, or the Fc effector silent EGFRxMet-IgG2σ (IgG2σ) decreased cell viability, confirming that these antibodies can inhibit AREG-induced proliferation (Fig. 3D, E and Supplementary Fig. 3F, G). IgG2σ was previously developed by engineering the EGFR and Met binding domains of amivantamab into an IgG2σ framework lacking the engagement of Fc receptors on immune cells[10,11]. Taken together, these results suggest that cells intrinsically expressing AREG (H292) or those engineered to overexpress AREG (H1703 and H838) rely on AREG-induced activation of EGFR for proliferation, and this can be blocked using AREG neutralizing antibody or amivantamab.

Amivantamab and AREG-neutralizing antibody reduce tumor growth in $EGFR^{WT}$ xenograft tumors

Following the observations that AREG induces in vitro proliferation of NSCLC cell lines, we assessed the role of AREG in driving tumor growth of two $EGFR^{WT}$ NSCLC xenograft models (H292 and LXFA-677). Mice harboring H292 cell-derived tumor xenograft (CDX) were treated with AREGB2, amivantamab, EGFRxMet-IgG2σ, or IgG1 isotype control antibodies, and tumor growth was measured over time. Both amivantamab and IgG2σ displayed similar tumor growth inhibition (ΔTGI (Day 28) = 111–113%; $^{***}P < 0.001$; Fig. 4A; Supplementary Fig. 4A shows individual animals), suggesting that an Fc domain capable of interacting with Fc-receptors is dispensable for amivantamab activity in this model. Notably, AREGB2 similarly inhibited tumor growth (ΔTGI = 106%; $^{***}P < 0.001$) with no statistically significant differences in tumor growth inhibition between targeting the ligand (AREG) with AREGB2 or the receptor (EGFR) with amivantamab/IgG2σ. Despite the cross-reactivity of AREG2B to mouse AREG, no weight loss or adverse signs were observed with any of the therapies evaluated (Supplementary Fig. 4B).

In parallel, the anti-proliferative efficacy of these compounds was assessed against a NSCLC PDX model, LXFA-677, which expresses $EGFR^{WT}$ and Met^{WT}. Similar to the H292 CDX model, treatment with amivantamab and IgG2σ resulted in complete tumor regressions (ΔTGI (Day 29) = 112%; $^{***}P < 0.001$; Fig. 4B; Supplementary Fig. 4C shows individual animals). Consistent with the results obtained with the H292 CDX mouse model, treatment with AREGB2 also led to a strong anti-tumor effect with a ΔTGI = 78% ($^{***}P < 0.001$). None of the treatments led to body weight loss (Supplementary Fig. 4D). However, contrary to the H292 CDX model, targeting EGFR through either amivantamab or IgG2σ led to a more substantial anti-tumor effect when compared to treatment with AREGB2 ($^{*}P < 0.05$) in this PDX model.

Our previous xenograft studies performed in $EGFR^{MUT}$ or Met^{AMP} human xenograft mouse models demonstrated that amivantamab-induced trogocytosis reduced phosphorylated and total levels of EGFR and Met[4,10,11]. To assess the role of amivantamab-induced trogocytosis in $EGFR^{WT}$ NSCLC PDX (LXFA-677), the targeted receptor levels and downstream signaling from tumor lysates collected 24 h after the first and second antibody doses were quantified by western blotting. As expected, the results showed that targeting either the receptors ($EGFR^{WT}$ and MET^{WT}) or ligand (AREG) reduced the levels of phosphorylated EGFR, Erk, and S6 (Fig. 4C and Supplementary Fig. 4E [24 h post-first dose] and Supplementary Fig. 4F, G [24 h post-second dose]). Interestingly, amivantamab and Fc-silent antibody (IgG2σ) treatment led to similar/minimal levels of EGFR and Met levels. These results suggest that trogocytosis is not a significant mechanism of action in this model with unaltered EGFR and Met.

Furthermore, we demonstrated that in samples with anti-tumor activity, there was reduced production or induced degradation of EGFR ligands. In this experiment, ELISAs from protein lysates prepared from harvested tumors, showed that the levels of AREG and HB-EGF, but not EREG, were significantly reduced in some of the tumors from antibody-treated animals compared to isotype control treatment (Supplementary Fig. 4H). Together, these results suggest that in these 2 $EGFR^{WT}$ tumor models, AREG plays a role in driving tumor growth, and amivantamab efficiently averts AREG-stimulated growth in an Fc-independent function.

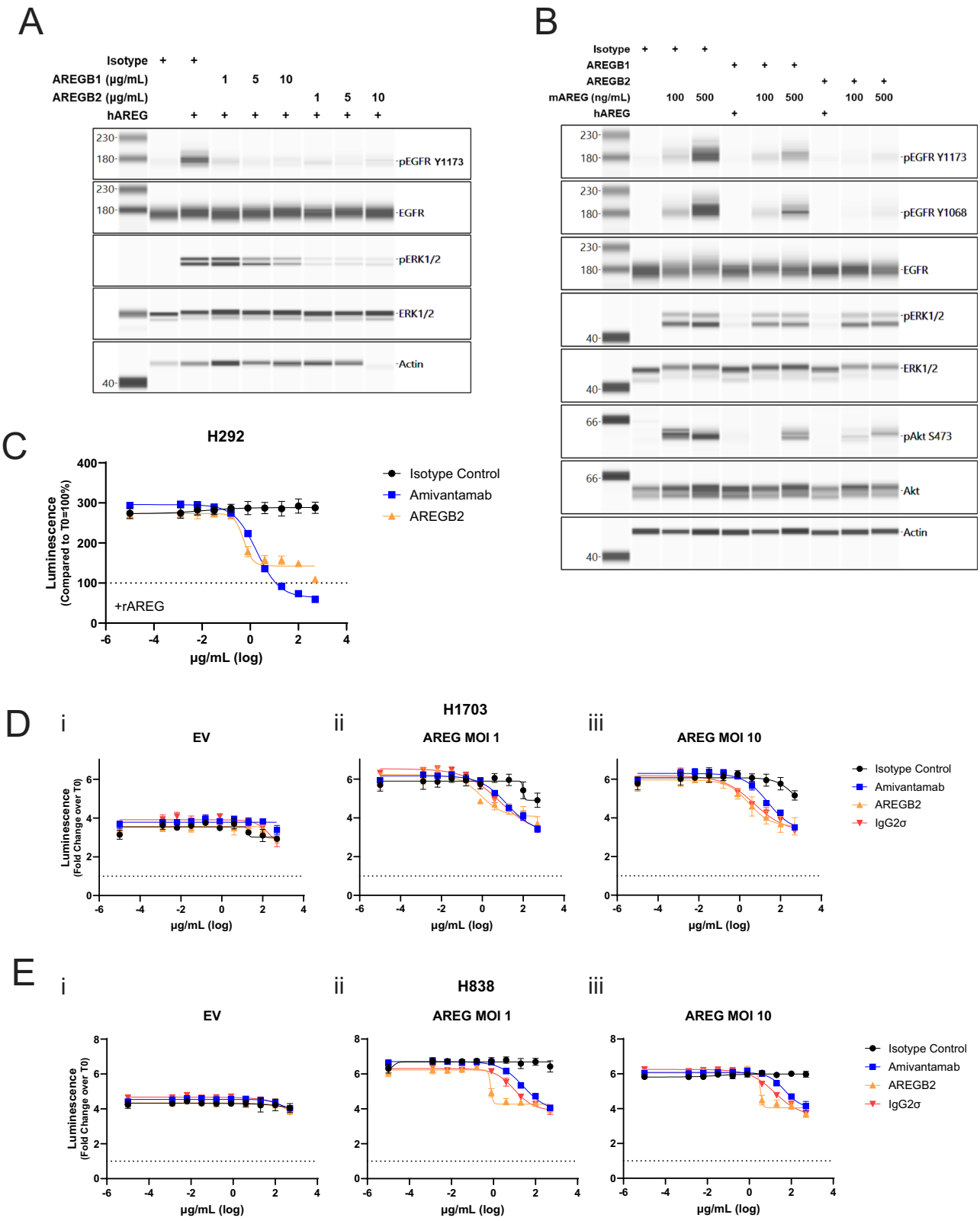

AREG RNA expression correlates with amivantamab anti-tumor activity in EGFR^{WT} NSCLC PDX models

To expand on the role of AREG and amivantamab on EGFR^{WT}/MET^{WT}NSCLC, the anti-tumor efficacy of amivantamab and IgG2σ were assessed against 11 and 10 PDX mouse models, respectively. Consistent with the results shown in Fig. 4, amivantamab treatment resulted in an efficacious (>60% TGI) anti-tumor activity in 5 of the models tested (Fig. 5A and Supplementary Fig. 5A). Notably, the Fc effector silent, IgG2σ, showed similar efficacy as amivantamab with no statistical differences between these 2 treatments ($P = 0.637$). Together, the data from this larger panel of EGFR^{WT} NSCLC PDXs shows that the enhanced Fc domain of amivantamab is dispensable, supporting the hypothesis that the ligand-blocking ability of amivantamab is the primary MOA in these tumor models.

Fig. 3 | Amivantamab and AREG-neutralizing antibodies block AREG-induced signaling and cell proliferation. A H292 cells were treated with a titration (1–10 μg/mL) of AREG-neutralizing antibodies AREGB1 (AR554) and AREGB2 (AR37), or 10 μg/mL of an IgG1 isotype control for five minutes in serum-free media. Cells were then stimulated with 100 ng/mL of recombinant human AREG (rhAREG) and harvested 15 min post-stimulation. Cells were lysed, and protein lysates were processed through capillary-based electrophoresis to quantitate levels of pEGFR^{Y1173}, EGFR, pErk1/2$^{T202/Y204}$, Erk1/2, and control actin. *The densitometry calculations for A are included in the* Supplementary Fig. 3A. **B** H292 cells were treated with 5 μg/mL of AREGB1, AREGB2, or 10 μg/mL of isotype control for five minutes in serum-free media. Cells were then stimulated with 100 ng/mL of rhAREG, or 100 and 500 ng/mL of recombinant mouse AREG and harvested 15 min post-stimulation. Cells were lysed, and protein lysates were processed through simple western to quantitate levels of pEGFR$^{Y1173/Y1068}$, EGFR, pErk1/2$^{T202/Y204}$, Erk1/2, pAkt^{S473}, Akt, and control actin. *The densitometry calculations for B are included in the* Supplementary Fig. 3B. **C** H292 cells were stimulated at days 0 and 3 with 100 ng/mL of rAREG and plated in 96-well plate. Cells in 1% FBS were treated with increasing concentrations of the IgG1 isotype control (black), amivantamab (blue), or AREGB2 (orange) for up to 6 days. Cell numbers on days 0, 3, and 6 were quantitated by CTG assay. The luminescence signals obtained at day 6 were normalized to their respective day 0 measurement (100%, dotted line). *Day 3 data are included in the* Supplementary Fig. 3D. H1703 (**D**) and H838 (**E**) cells previously transfected with EV **(i)** or AREG expressing lentivirus at MOI 1 **(ii)** or 10 **(iii)** (AREG-OE) were cultured at low-serum concentrations (1%) for up to six days in presence of increasing concentrations of IgG1 Isotype control (black), amivantamab (blue), EGFR/MET Fc-silent antibody (IgG2σ; red), or AREGB2 (orange). Cell numbers were quantitated by CTG to determine cell proliferation by comparing the luminescence signals obtained at day 6 with their respective day 0 measurement (dotted line). *Day 3 data are included in the* Supplementary Fig. 3F, G.

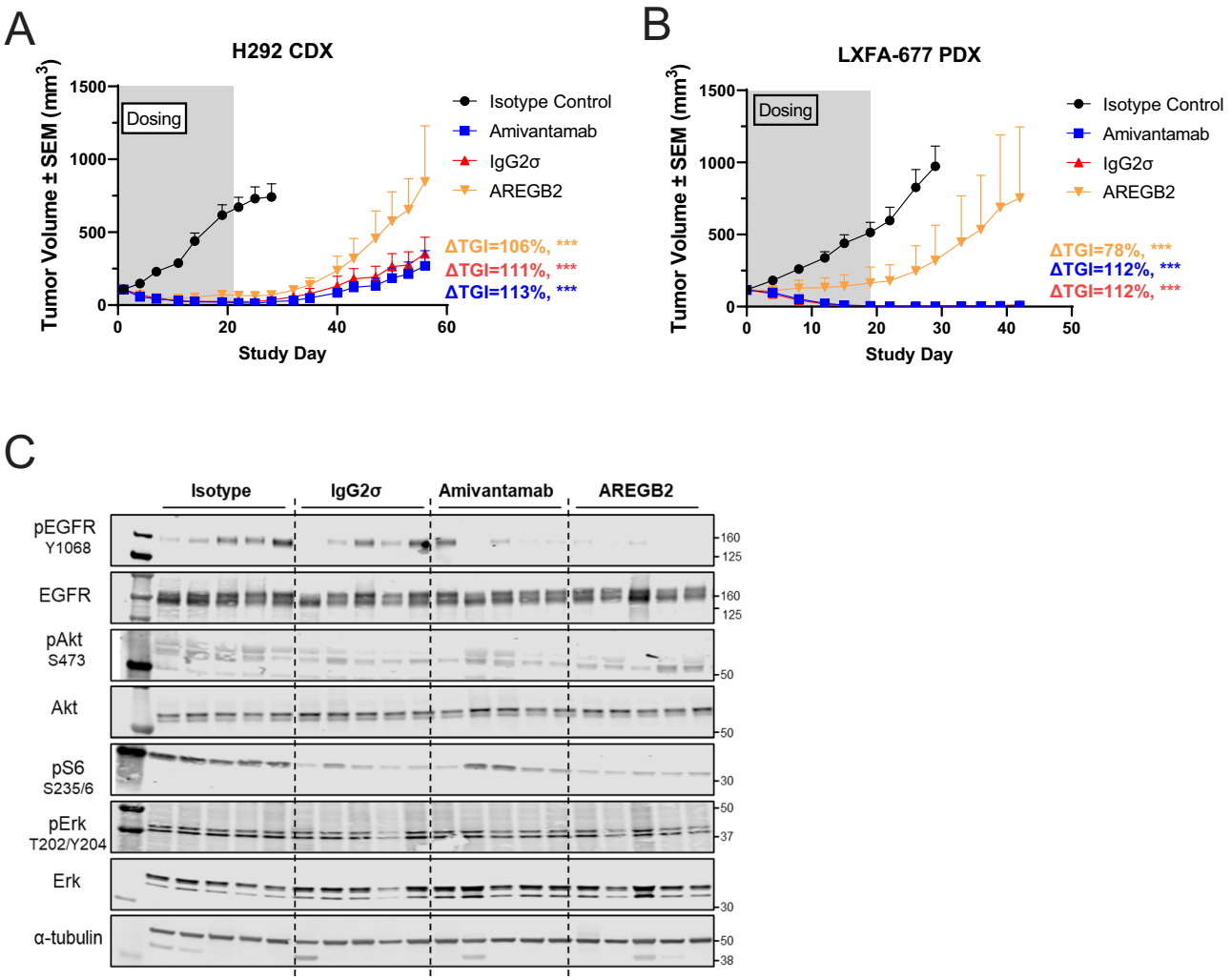

Fig. 4 | AREG is a driver of EGFR^{WT} tumor growth which is inhibited by amivantamab. The H292 (**A**) and LXFA-677 (**B**) non-small cell lung cancer (NSCLC) xenografts models were implanted subcutaneously in nude mice. After tumors reached 100–150 mm^3, mice were randomized into four arms and treated i.p. twice a week with 10 mg/kg of IgG1 Isotype control (black), amivantamab (blue), EGFRx-Met Fc-silent antibody (IgG2σ; red), or AREGB2 (orange) for 3 weeks (gray background). Tumor sizes were measured with caliper thrice per week. Change in tumor growth inhibition (ΔTGI) was calculated on days 28 (**A**) and 29 (**B**). Error bars represent the standard error of the mean. **C** Animals harboring the LXFA-677 tumors were treated for 24 h as in A, but tumor harvested immediately after animal euthanasia and snap-frozen in liquid nitrogen. Protein lysates were prepared from the tumors and subjected to western blotting for quantitation of pEGFR^{Y1068}, EGFR, pAkt^{S473}, Akt, pS6$^{S235/6}$, pErk1/2$^{T202/Y204}$, Erk1/2, and control α-tubulin. *P*-value was determined by Walt-type statistics, ***$P < 0.001$. *The densitometry calculations are included in the* Supplementary Fig. 4E.

To determine whether the expression levels of the EGF and Met receptors in these models were associated with amivantamab activity, tumors from these PDX models were subjected to immunohistochemistry and assessed for EGFR and Met expression and correlation to amivantamab efficacy (ΔTGI). The results show that in these models, the levels of EGFR or Met did not correlate with amivantamab efficacy (Supplementary Fig. 5B). These results suggest that in this set of models, neither the levels of EGFR nor Met predict sensitivity of the tumors to amivantamab.

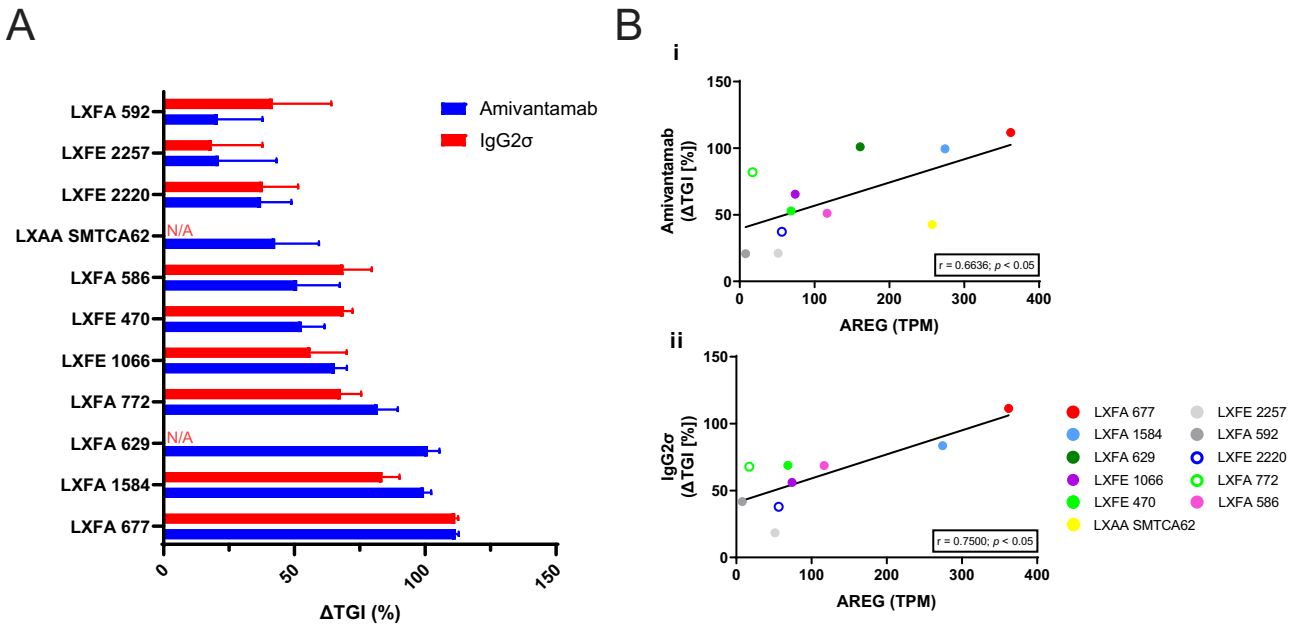

Fig. 5 | *AREG* level of expression correlates with amivantamab efficacy against EGFR^{WT} NSCLC PDX models independent of amivantamab Fc function. A Ten EGFR^{WT} NSCLC PDX models were established in mice and treated for 3-4 weeks twice a week with 10 mg/kg of either Isotype control, amivantamab, or IgG2σ. The ΔTGI (%) exerted by either amivantamab (blue) or IgG2σ (red) was calculated one week post treatment completion. *IgG2σ was not evaluated in the LXFA-629 model. The ΔTGI induced by IgG2σ in the LXAA-SMTCA62 model was found to be a significant outlier and excluded from the analysis.* Error bars represent the standard error of the mean. **B** Amivantamab **(i)** and IgG2σ **(ii)** ΔTGI (%) were determined against these NSCLC PDX models and plotted against EGFR ligand *AREG* RNA levels (transcripts per million, TPM) determined by RNAseq analysis. Spearman's correlation were calculated for ligand: treatment relationship.

Next, we sought to determine if amivantamab or IgG2σ efficacy correlated with expression of EGFR ligands. To do that, we evaluated the RNA levels of seven EGFR ligands from the tested PDX tumors and assessed whether their mRNA levels correlate to amivantamab and/or IgG2σ efficacy (ΔTGI; Fig. 5B and Supplementary Fig. 5C, D). Of the seven EGFR ligands, only AREG expression significantly correlated with amivantamab ($^*P < 0.05$) and IgG2σ ($^*P < 0.05$) efficacy. These results suggest that AREG expression is an important factor in the identification of models dependent on EGFR signaling and which are sensitive to AREG-blocking therapies, including amivantamab.

AREG level of expression is significantly higher in non-mutated versus mutated EGFR LUAD tumors

Leveraging the extensive human Cancer Genome Atlas (TCGA) data bank, we assessed the level of *AREG* expression in NSCLC tumors. We found that NSCLC patients with gains or amplification of EGFR copy numbers showed significantly higher levels of *AREG* expression than diploid NSCLC tumors (Fig. 6A). Importantly, following NSCLC subtype analysis, the significance remains in lung adenocarcinoma (LUAD) patients. However, contrary to the results from LUAD, gains or amplifications of EGFR copy numbers in squamous cell carcinoma (LUSC) tumors do not have higher levels of *AREG* expression than those with diploid copy number. Similarly, we found that LUAD tumors with a non-mutated EGFR status showed significantly higher levels of *AREG* expression that patients carrying EGFR mutations (in-frame, missense, splice, and truncating; Fig. 6B). Lastly, we explored mutual exclusivity between tumors carrying EGFR mutations and those with the highest levels of *AREG* RNA levels. The analysis shows that 1 out of 46 (2%) LUAD tumors with an *AREG* Z-score > 1.3 carried EGFR mutations, while none of the other 64 LUAD tumors with EGFR mutations was deemed as a high AREG expressors (98.4%) (Fig. 6C and Supplementary Fig. 6A, B). These results demonstrate a significant association of mutual exclusivity (Log2 Odds Ratio: −2.873; *q*-value, 0.019). Similar to LUAD, out of 466 LUSC patients' tumors, 17 were identified as high (Z-score >1.3) AREG expressors and none of them carried EGFR mutations. Although these results were not statistically significant, the analysis shows a trend towards mutual exclusivity (Log2 Odds Ratio: −3). Thus, the broader analysis of the TCGA data from NSCLC patients supports our hypothesis suggesting that in LUAD patients, elevated levels of *AREG* mRNA occur in the absence of EGFR mutations most likely resulting in EGFR activation, increased signaling and potentially leading to tumorigenesis. Altogether, these data indicate that AREG expression may be a predictive biomarker of amivantamab clinical activity in EGFR^{WT} NSCLC patients.

Discussion

The efficacy of amivantamab against NSCLC EGFR^{MUT} tumors has been demonstrated preclinically[4,10,11] and clinically with the approval of Rybrevant® in mutant EGFR^{ex20ins} NSCLC and the positive phase III clinical results against common EGFR^{MUT} NSCLC[6–9]. In addition, previous preclinical studies demonstrated amivantamab efficacy against NSCLC tumor models with unaltered EGFR and Met[4]. Considering the multiple context-dependent mechanisms of action of amivantamab against EGFR^{MUT} NSCLC[4,10], including ligand blocking, receptor internalization, and trogocytosis, we assessed which of these mechanisms may be predominant in NSCLC tumor models lacking EGFR and/or Met activating mutations, and whether the EGFR ligands could play a role in driving tumor growth in these EGFR^{WT} tumors. We first explored factors that may drive EGFR signaling in tumor cells lacking EGFR-activating mutations. Among the seven known EGFR ligands, we identified AREG as the most abundant ligand in NSCLC patient tumors, with higher expression in the circulation of NSCLC patients than in healthy volunteers. AREG binding to EGFR has been reported to drive many tumorigenic processes, such as cell proliferation, migration, invasion, and inhibition of apoptosis[19,20]. AREG provides growth signals in multiple cell types, including those originating from the liver, colon, pancreas, stomach, and lung[19–21]. In this study, we demonstrated that AREG induces the proliferation of NSCLC cells and that both amivantamab and an AREG-targeting antibody inhibit ligand-induced cell signaling and proliferation.

Additionally, we showed that the AREG-targeting antibody, AREGB2, is highly effective in reducing the growth of NSCLC tumors. These observations suggest that ligands, particularly AREG, might contribute to tumor

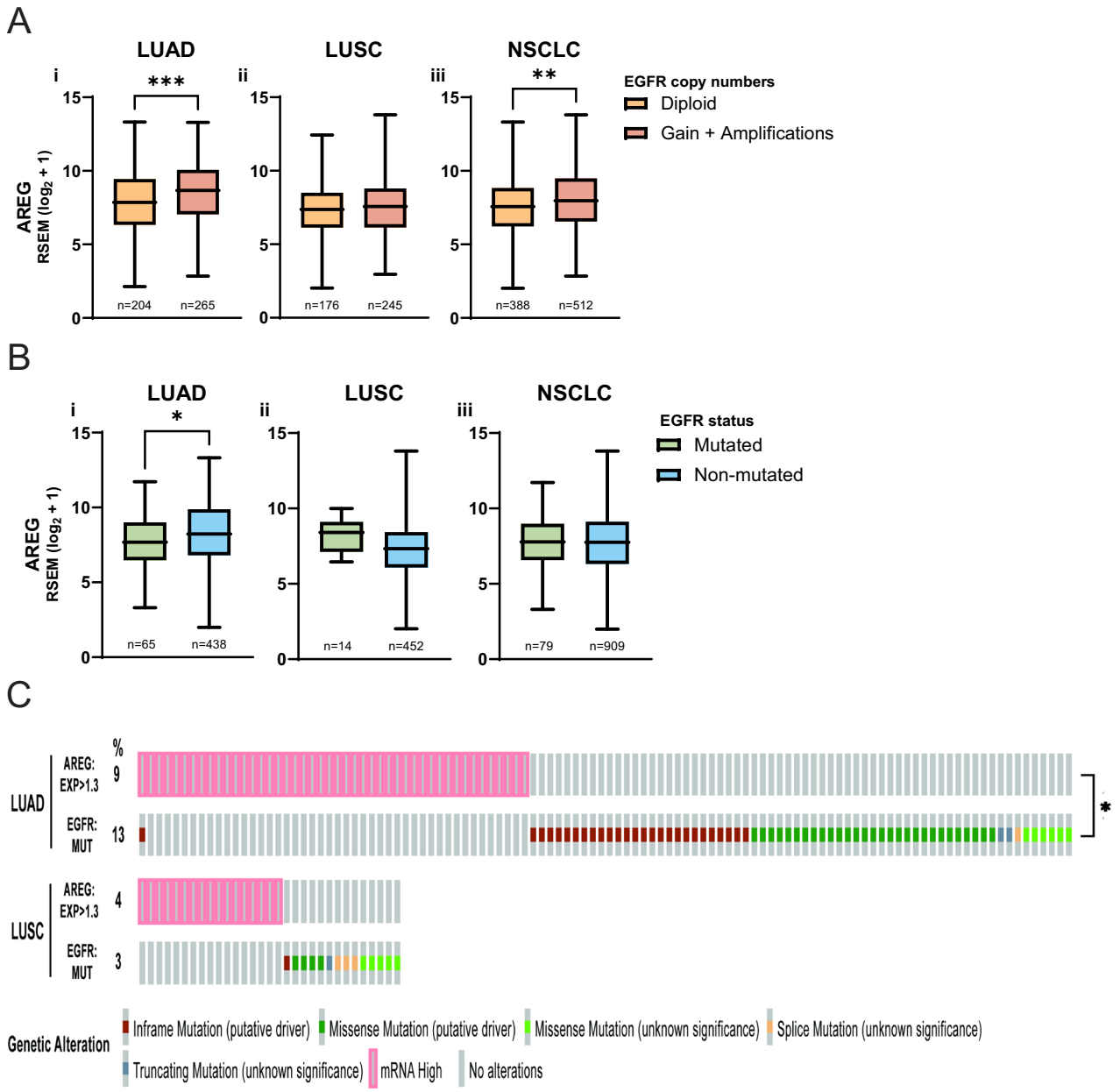

Fig. 6 | High *AREG* expression is mutually exclusive to EGFR aberration in NSCLC and *AREG* expression is significantly higher in EGFR^{WT} versus mutated in LUAD. The *AREG* RNA expression (RSEM) of NSCLC patients available from TCGA was graphed according to EGFR copy number (**A**) and status (**B**). *P*-values were determined by unpaired Student's *t*-test, $*P < 0.05$; $**P < 0.01$; $***P < 0.001$. Box-and-whisker plots represents min-to-max distribution with center lines at the median. **C** Oncoprints displays the patients with the highest levels of AREG expression (Z-score >1.3) and the mutational landscape for EGFR in LUAD and LUSC patients. *P*-value was determined by Fisher's Exact test, $* P < 0.05$.

growth in NSCLC models with unaltered EGFR and Met by activating the EGFR signaling cascade. Our studies primarily focused on the most abundant EGFR ligand from the analyzed NSCLC samples, AREG. However, since amivantamab binds to the ligand-binding epitope on EGFR, we hypothesize that our observations with AREG may extend to all EGFR ligands[4].

In addition to the activation of the signaling pathway elicited by the EGFR ligands, activation of Met via either genetic aberrations or interaction with its ligand, HGF, might increase pro-oncogenic processes such as cell proliferation, invasion, survival, and angiogenesis[3]. HGF induces Met activation in tumors through autocrine and paracrine mechanisms. In lung cancers, HGF is mainly produced by mesenchymal cells and fibroblasts[15]. However, in xenograft mouse models, where the tumor microenvironment (TME) is of murine origin, mouse HGF does not bind and activate human Met on tumors, suggesting that in the models used in these experiments with Met^{WT} (not gene amplified), the role of Met signaling is likely not fully representative of human tumors[16]. Therefore, our data suggest that the dominant anti-tumor activity exerted by amivantamab in these xenograft tumor models is through the blockade of EGFR signaling.

In tumors driven by EGFR ligands, receptor blockade would be a reasonable therapeutical approach as it would prevent ligand-induced signaling[22]. Indeed, we demonstrated that in EGFR^{WT} NSCLC PDX tumors, *AREG* levels correlate with amivantamab efficacy, whereas EGFR and Met expression did not correlate to amivantamab anti-tumor activity. Contrary to amivantamab efficacy in EGFR^{MUT} NSCLC[4,10], we demonstrated that in unaltered EGFR and Met NSCLC models, the active Fc-domain of

amivantamab was not required for efficacy. These observations suggest that in tumors driven by EGFR ligands, the ligand-blocking function of amivantamab is sufficient to inhibit tumor growth. These results suggest that different MOAs of amivantamab are at play depending on the genetic profile of the tumors. For instance, in tumors driven by mutant EGFR or Met, increased amivantamab efficacy is observed compared to that with a variant of amivantamab with reduced Fc-function (IgG2σ), demonstrating the requirement of antibody-dependent processes involving immune cells, such as trogocytosis, for maximal amivantamab anti-tumor activity in these models. Conversely, the ligand-blocking function of amivantamab is sufficient (similar efficacy between amivantamab and that with reduced Fc-function) to inhibit tumor growth in unaltered EGFR and Met NSCLC xenograft models. Interestingly, this immune-independent MOA might suggest a role for amivantamab in patients with a weakened immune system or against low immune infiltrated (cold) tumors[23,24]

In addition to AREG's role in the proliferation and survival of tumor cells, an autocrine and paracrine role for AREG in modulating the TME has been proposed[25]. AREG is expressed/secreted from several immune cells, including neutrophils, $CD8^+$ T cells, regulatory T cells (Treg), and macrophages, which have also been shown to modulate signaling in these immune cells[25–28]. Further, AREG enhances the suppressive capacities of Treg over $CD4^+$ and $CD8^+$ T cells, and macrophage-secreted AREG reduces Th1 cell activation while increasing Treg differentiation[26,27]. Furthermore, AREG plays an essential role in tissue homeostasis as AREG secreted from Treg and macrophages is essential for tissue injury repair, including the lung[29,30]. In addition to the oncogenicity of stromal-secreted AREG on tumors, it also induces PD-L1 expression, leading to reduced anti-tumor immunosurveillance[31]. Thus, it would be interesting to explore whether AREG-blocking therapies could enhance the anti-tumor action exerted by immune checkpoint inhibitors (e.g., pembrolizumab), which are approved for NSCLC patients[32]. Altogether, these studies highlight AREG as a multifunctional protein that enhances the proliferation of the tumor cells while reducing immune cell fitness in the TME.

The correlation between tumor AREG level in NSCLC and sensitivity to EGFR inhibition, such as EGFR TKI or cetuximab[12], has also been explored in colorectal cancer (CRC); however, with conflicting conclusions. Several studies demonstrated that high *AREG* and/or *EREG* mRNA levels in RAS^{WT} metastatic/advanced CRC correlate with improved cetuximab[13,14,17] or panitumumab[33] treatment responses. Similarly, in a cohort of CRC patients treated with cetuximab, those with high AREG and low heregulin (neuregulin) protein levels in the plasma showed better progression-free and overall survival[34].

In contrast to these studies, Kim et al. demonstrated that in CRC patients treated with cetuximab plus FOLFIRI, high AREG levels in plasma were associated with an inferior progression-free survival (PFS) compared to low-expressing patient population[35]. Similarly, in HER2-positive breast cancer patients treated with trastuzumab plus taxane, serum levels of AREG were associated with a shorter PFS[36]. Both studies suggested that AREG expression led to Akt and Erk pathway activation, circumventing the inhibition induced by cetuximab or trastuzumab[35,36]. Furthermore, high AREG expression from primary CRC tumors or circulating in the serum of patients was suggested to be related to liver and peritoneal metastases and worse outcomes[37,38]. Moreover, in two reports, expression of AREG in NSCLC patients was linked to poorer outcomes following treatment with erlotinib or gefitinib[39,40]. The discrepancies between these studies could be due to multiple factors, including but not limited to the patient populations (e.g., prior lines of treatment, genetic status of additional oncogenic drivers, stage of disease), the source of the specimen (e.g., plasma, tumor) analyzed, the method used (mRNA vs protein) or a combination of the above. Future prospective studies are needed to assess the translatable validity of ligands as a biomarker of patient response to anti-EGFR treatments.

Based on current and prior studies, targeting AREG could be considered a viable therapeutic approach against EGFR/Met wild-type tumors expressing high levels of AREG[18,41–44]. However, given the multitude of EGFR ligands, targeting AREG alone might not lead to efficacy in other EGFR-ligand-driven tumors and could lead to the development of resistance through compensatory mechanisms mediated by the other EGFR ligands[45]. Supporting this hypothesis, our results presented here showed that AREGB2 does not completely block LXFA-677 tumor growth, suggesting that, in this model, targeting AREG is not sufficient for complete tumor growth inhibition.

The results presented in our studies highlight amivantamab (EGFR and Met bispecific antibody) as a superior treatment option to block the oncogenic activity of AREG and likely other EGFR ligands while also blocking Met signaling, the common mechanism of resistance of EGFR inhibition. Altogether, these reported studies highlight AREG as a potential predictive biomarker of activity and support ongoing clinical trials assessing amivantamab efficacy in altered EGFR or Met cancers as well as cancers with unaltered EGFR and Met.

Methods

Cell Lines

The NCI-H292 (H292), NCI-H1703 (H1703), and NCI-H838 (H838) cells were acquired from the American Type Culture Collection (ATCC) and maintained in GlutaMAX™-RPMI 1640 (Gibco) supplemented with 10% heat-inactivated Fetal Bovine Serum (FBS; Gibco) in a humidified incubator at 37 °C, in an atmosphere of 5% CO_2 and 95% air. The specific catalog number for the reagents are available in Supplemental Table 1. The cells were regularly authenticated and subjected to mycoplasma testing.

Ligand stimulation

For ligand-stimulation assays, cells were seeded in the appropriate media containing 1% FBS and allowed to adhere overnight. Before the stimulation, cells were washed with PBS and starved for up to 3 h in FBS-free media before treatment with the ligands in the presence or absence of the inhibitory compounds. All the recombinant proteins in a lyophilized format were acquired from Peprotech (Thermo Fisher) or R&D Systems and resuspended and stored as recommended by the manufacturer.

Plasmids and Lentiviral Infection

To establish AREG overexpressing cells, H838 and H1703 cells were transduced with lentiviruses containing a myc-tagged-hAREG-transgene under the control of the EF1α promoter (VectorBuilder). The respective lentivirus packaged with a non-coding sequence was also used as an empty vector control (EV). The infection was performed through standard spinfection protocols. Briefly, cells were detached with TrypLE (Gibco), and 125,000 cells were plated in each well of a 12-well plate. 1.25×10^5 and 1.25×10^6 viral particles were added to the cells for a multiplicity of infection (MOI) of 1 or 10, respectively. These MOIs were used to achieve different levels of expression given the varying levels reported in $EGFR^{WT}$ cell lines[12]. To enhance transduction, the viral-cell mixture was supplemented with polybrene (8 μg/mL; VectorBuilder) and spun for 90 min at 2000 RPM at 30 °C. After centrifugation, the plates were incubated overnight at 37 °C in an atmosphere of 5% CO_2 and 95% air. The following day, cells were washed twice with PBS, and fresh media was added supplemented with 1 μg/mL of puromycin (Gibco). After cells were selected and expanded, H1703 and H838 cells were maintained in media containing 0.5 and 1 μg/mL of puromycin, respectively.

In vivo studies

All animal experiments were performed according to the protocols approved by the appropriate Institutional Animal Care & Use Committee at Janssen Research & Development and Charles River Laboratories.

Cell-derived xenograft

Ten million H292 cells in 50% Matrigel™ (BD Biosciences) were subcutaneously implanted in female NCr nu/nu mice (Charles River Laboratories). Once tumors reached an average of 108.6 mm^3 in size, they were randomly sorted into four bins and treated with low-fucose isotype, amivantamab, EGFRxMet-IgG2σ, and AREGB2. All treatments were

performed intraperitoneally at a dose of 10 mg/kg. As a prophylaxis, animals were given DietGel from the first day of dosing. Tumor growth was tracked by caliper measurement thrice weekly. The tumor size in mm^3 was calculated from: Tumor Volume = $(w^2 \times l)/2$, where 'w' = width and 'l' = length, in mm, of the tumor. The % ΔTGI was calculated as %ΔTGI = (1−[mean(TVT) − mean(TVT0]/[mean(TVC) − mean(TVC0)]) × 100; where 'TVC' = tumor burdens of the control group at a given day, 'TVC0' = tumor burdens of the control group at the initiation of treatment, 'TVT' = tumor burdens of the treatment group at a given day, and 'TVT0' = tumor burdens of the treatment group at the initiation of treatment.

Patient-derived xenograft

The tumor fragments from the patient-derived NSCLC xenografts were subcutaneously implanted in female NMRI nu/nu mice (Charles River Laboratories). For the efficacy study, once the tumors reached an average of 100–150 mm^3, the animals were divided into four treatment groups of 8–10 subjects per group. The low-fucose isotype control, amivantamab, EGFRxMet-IgG2σ (IgG2σ), and AREGB2 were administered intraperitoneally twice weekly at 10 mg/kg for 3 weeks. Tumor growth was tracked by caliper measurement thrice weekly, and tumor sizes were determined as mentioned above. For the pharmacodynamics arm of the LXFA-677 study, once tumors reached an average of 223.1–244.8 mm^3, animals were randomly assigned into four treatment groups. Tumor samples from five animals per group were collected 24 h after the first and second doses.

Immunohistochemistry and the respective quantification for EGFR and Met was performed by CellCarta (previously Mosaic Laboratories LLC).

Western Blots

Protein lysates were prepared by incubating cells for 10 min at 4 °C with Radioimmunoprecipitation assay (RIPA; Thermo Fisher) buffer supplemented with 50 U/mL of Benzonase Nuclease (Sigma-Aldrich) and 1x HALT protease/phosphatase cocktail (Thermo Fisher) or 1 tablet of Phospho-Stop (Sigma-Aldrich) and cOmplete Protease inhibitor cocktail (Sigma-Aldrich) per 10 mL of buffer. Lysates were clarified by centrifugation at 14000 RPM for 10 min at 4 °C. The protein concentrations were determined through Pierce BCA Protein Assay (Thermo Fisher).

For traditional western blots, the proteins were resolved through SDS-PAGE (Thermo Fisher) and transferred to 0.2 µM nitrocellulose membranes (Thermo Fisher). After the transfer of the proteins, the membranes were blocked for at least 1 h at room temperature with Odyssey Blocking Buffer (Tris-buffered saline, TBS, LI-COR Biosciences). Membranes were incubated with the appropriate primary antibodies diluted in TBS containing 0.1% Tween-20 (TBST) overnight at 4 °C. After the overnight incubation, membranes were washed thrice for 10 min each with 0.1% PBS-Tween 20 (PBST) and incubated for 1 h at room temperature with the secondary antibodies diluted in TBST. Before imaging, membranes were washed thrice for 10 min each with 0.1% PBST. The membranes were imaged in an Odyssey DLx Imaging System (LI-COR Biosciences). The densitometry analysis was performed manually in Image Studio Lite software (Ver 5.2; LI-COR Biosciences) by normalizing the protein of interest to their respective loading control (e.g., (pEGFR/actin)/(EGFR/actin)). The list of the antibodies used in this study can be found in the Supplemental Table 1.

For capillary-based electrophoresis (Simple Western™), protein lysates were prepared according to the manufacturer protocols to a 0.05–0.5 mg/mL concentration and processed in the SallySue or Jess Imaging System (Biotechne). The results were visualized, and the densitometry (Peak Area) was calculated through the SW Compass Software (Ver 5.0.1 and 6.3; Biotechne). The densitometry was determined by normalizing the protein of interest to their respective loading control.

The LXFA-677 tumors were harvested immediately after euthanasia and snap-frozen in liquid nitrogen. Frozen samples were pulverized (Covaris CP02 CryoPREP) and lysed in RIPA (Thermo Fisher) buffer supplemented with 2x HALT protease/phosphatase cocktail (Thermo Fisher). Lysates were processed further through 20 cycles of 10 s per cycle in a water-bath sonicator (Covaris E220 Evolution). The protein clarification, BCA, and SDS-PAGE were performed as above. Membranes were transferred to 0.2 µM nitrocellulose and blocked for at least 1 h at room temperature with Odyssey Blocking Buffer (TBS) before incubating them with the appropriate primary antibodies overnight at 4 °C.

Human samples and protein quantification

The NSCLC patient tumor and serum samples were acquired from BioIVT and Analytical Biological Services Inc. These samples were collected from studies with reference numbers APP0317, APP0460, APP0425, and APP0823 and were reviewed and approved by the Ethics Commission. Healthy volunteer samples were obtained from the Janssen Spring House Employee Donor Program reviewed by Advarra Institutional Review Board (STUDY ID: NOCOMPOUNDNAP1001). All specimens (healthy and diseased) were collected after obtaining informed consent.

Pieces of fresh frozen tumor tissues for protein extraction were collected on dry ice and homogenized using Tissue Extraction Reagent I (Thermo Fisher) with added Protease and Phosphatase Inhibitor Mini Tablet (Thermo Fisher) at a ratio of 10 µL buffer per mg of tissue. Tissue lysates were cleared by centrifugation at maximum speed for 10 min at 4 °C. Protein concentration was measured by BCA assay (Thermo Fisher), and samples were adjusted to a final concentration of 1 mg/mL for subsequent Luminex and ELISA analyses.

Ligand levels of EGFR and Met were measured by Luminex assays at Rules-Based Medicine Inc. AREG, EGF, EREG, and HB-EGF were measured by the HCANCER2 panel. BTC was measured by the HMPC18 and HMPC51 panels, respectively. Samples below the assay range are plotted at the lower limit of quantification. TGFα was measured in serum and tumor lysates using ELISA kits (R&D Systems).

ELISA

An equal number of cells were plated and allowed to grow overnight in RPMI 1640 supplemented with 1% FBS. Then, the supernatant was collected, spun down at 2500 RPM for 10 min, and filtered through a 0.45 µm filter (Millipore) to create a cell-free conditioned media. Samples were diluted as needed, and AREG was measured according to the manufacturer's protocol (Invitrogen or R&D Systems).

To measure ligand levels from the PDX tumors, lysates were prepared and diluted to 160 µg/mL. According to the manufacturer's protocols, TGFα, EREG, and HB-EGF were measured in serum and tumor lysates using ELISA kits (R&D Systems and RayBiotech). Samples below the assay range are plotted at the lower limit of quantification.

AlphaLISA

Ten thousand H292 cells were seeded per well in a 96-well plate and incubated overnight in RPMI-1640 containing 1% FBS. For testing amivantamab-mediated blockade of EGFR, cells were serum-starved for 1 h and then treated for an additional hour with increasing concentrations of amivantamab or an isotype control in a total volume of 45 µL/well. After the incubation, cells were stimulated with 5 µL of rAREG (final concentration of 1000 ng/mL) for 15 min. After incubation, samples were washed with PBS twice and lysed in 50 µL/well of 1x AlphaLISA lysis buffer (Revvity). Samples were shaken for 10 min and either stored at −20 °C until the assay was completed or processed immediately. All treatment were done in the absence of serum. Thirty microliters of the lysates were transferred to a 96-well white half-area clear-bottom plate. The positive control was resuspended in water and diluted 1:10. The plate was incubated with the acceptor beads for 1 h at room temperature and then overnight at room temperature with the donor beads. All the incubations and sample preparations were performed while protected from light, as recommended by the manufacturer. The bottom of the plate was covered, and the samples were measured at 545 and 615 nm in an Envision Plate Reader (Revvity).

For testing additional compounds and ligands, the assays were performed as above with a few changes. Briefly, 20,000 H292 cells were seeded per well in a 96-well plate and incubated overnight in RPMI-1640

containing 1% FBS. The next day, cells were serum-starved for 1 h and then treated for an additional hour with 10 μg/mL of either low-fucose IgG isotype, amivantamab, or AREGB2, in a total volume of 45 μL/well. After the incubation, cells were stimulated with 5 μL of rAREG, rhEGF, and r-mouse(m) AREG (final concentration of 100 ng/mL) for 15 min.

Cell proliferation assays

Two thousand five hundred cells were plated in each well of 96-well white flat bottom plates in 100 μL of 1% FBS-containing RPMI 1640. For the cells stimulated with the ligands, 24 h after plating, cells were treated with rAREG at the indicated concentrations and incubated for up to 6 days in the presence or absence of low-fucose isotype, amivantamab, αEGFR single arm (EGFR x RSV), αMet single arm (Met x RSV), IgG2σ, or AREGB2. For the cells overexpressing AREG, equal numbers of cells were plated as above and treated with the compounds for up to 6 days. To determine cell proliferation, cells were incubated with 75–100 μL of CellTiter-Glo 2.0 (Promega) according to the manufacturer protocols, and luminescence was measured with an Envision Plate Reader. Additional plates with cells were measured at day 0 (24 h post-plating; before ligand stimulation) to use as base levels to calculate the fold change over time.

Dimerization assay

The EGFR dimerization assay was acquired from Eurofins DiscoverX and performed according to the manufacturer's protocol. Briefly, U20S cells were thawed and plated in 96 well white, clear bottom plates with the provided cell plating (CP) Media. Cells were incubated for 24 h at 37 °C + 5% CO_2. To evaluate AREG-induced dimerization, the next morning, cells were treated with a 3-fold titration (0.3–20,000 ng/ml) of rAREG and incubated for 5 h at 37 °C + 5% CO_2. To evaluate the ability of amivantamab in blocking AREG-induced dimerization, cells were prepared as above but treated for 1 h with increasing concentrations of amivantamab or an isotype control. After the incubation, 5 μL of AREG were added to the plate for a final concentration of 1000 ng/ml and incubated for 5 h at 37 °C + 5% CO_2. After the incubations the media containing rAREG was removed from the wells and 100 μL of fresh CP media was added to respective well followed by 110 μL of the PathHunter Flash Detection Reagent. Cells were incubated with the detection reagent for 1 h at RT and protected from light. After incubation, luminescence was measured with a EnVision Nexus Plate Reader (Revvity).

The Cancer Genome Atlas

Analysis of the TCGA data was done through cBioPortal[46–48]. The data included 487 samples from Lung Squamous Cell Carcinoma (TCGA, PanCancer Atlas) and 566 samples from Lung Adenocarcinoma (TCGA, PanCancer Atlas).

Statistics

All the graphs and statistical tests were performed on Prism GraphPad version 9 and 10, or in R[49]. For mutual exclusivity, a Fisher's test was conducted. Student's t-tests were used to compare the difference in ligand levels of NSCLC patients versus healthy volunteers and for the TCGA analysis. For samples with values below the lower limit of quantification, a Tobit regression analysis was performed. Two-way ANOVAs with Dunnett's multiple comparison tests were used to calculate the effect of ligands in promoting cell proliferation over time. For animal studies, percent changes in baseline-corrected mean tumor burdens were assessed using % ΔTGI. A two-sided hypothesis test was used to compare % Δ TGI to 0. Specifically, a Wald-type statistic was compared to a Student's *t*-distribution with degrees of freedom calculated using the Satterthwaite approximation. The variance was estimated using the delta method, assuming mean tumor burdens were normally distributed. Kruskall-Walli's with Dunn's multiple comparison tests were used to determine differences in protein levels imaged through capillary-based western blotting and measured by ELISA after 2 or 5 days of treatment. The same set of PDX models were treated with either of two molecules, and a paired Student's *t*-test was used to determine whether there was a difference in the average tumor volumes. Finally, according to Grubb's test, one PDX model (LXAA-SMTCA62) was excluded from a set of analyses as determined to be an outlier. All error bars represent the standard deviation unless otherwise specified.

Data availability

RNA data from the PDX models is available from Charles River Laboratories. TCGA data was obtained from cBioPortal[46–48].

Received: 19 January 2024; Accepted: 28 August 2024;
Published online: 06 September 2024

References

1. Herbst, R. S., Morgensztern, D. & Boshoff, C. The biology and management of non-small cell lung cancer. *Nature* **553**, 446–454 (2018).
2. Singh, B., Carpenter, G. & Coffey, R. J. EGF receptor ligands: recent advances. *F1000Res* **5**, 2270 (2016).
3. Zhang, Y. et al. Function of the c-Met receptor tyrosine kinase in carcinogenesis and associated therapeutic opportunities. *Mol. Cancer* **17**, 45 (2018).
4. Moores, S. L. et al. A Novel Bispecific Antibody Targeting EGFR and cMet Is Effective against EGFR Inhibitor–Resistant Lung Tumors. *Cancer Res.* **76**, 3942–3953 (2016).
5. Neijssen, J. et al. Discovery of amivantamab (JNJ-61186372), a bispecific antibody targeting EGFR and MET. *J. Biol. Chem.* **296**, 100641 (2021).
6. Park, K. et al. Amivantamab in EGFR Exon 20 Insertion–Mutated Non–Small-Cell Lung Cancer Progressing on Platinum Chemotherapy: Initial Results From the CHRYSALIS Phase I Study. *J. Clin. Oncol.* **39**, 3391–3402 (2021).
7. Zhou, C. et al. Amivantamab plus Chemotherapy in NSCLC with EGFR Exon 20 Insertions. *N. Engl. J. Med.* **389**, 2039–2051 (2023).
8. Passaro, A. et al. Amivantamab plus chemotherapy with and without lazertinib in EGFR-mutant advanced NSCLC after disease progression on osimertinib: primary results from the phase III MARIPOSA-2 study. *Ann. Oncol.* **35**, 77–90 (2023).
9. Cho, B. C. et al. Amivantamab plus lazertinib in osimertinib-relapsed EGFR-mutant advanced non-small cell lung cancer: a phase 1 trial. *Nat. Med.* **29**, 2577–2585 (2023).
10. Vijayaraghavan, S. et al. Amivantamab (JNJ-61186372), an Fc Enhanced EGFR/cMet Bispecific Antibody, Induces Receptor Downmodulation and Antitumor Activity by Monocyte/Macrophage Trogocytosis. *Mol. Cancer Therapeutics* **19**, 2044–2056 (2020).
11. Grugan, K. D. et al. Fc-mediated activity of EGFR x c-Met bispecific antibody JNJ-61186372 enhanced killing of lung cancer cells. *MAbs* **9**, 114–126 (2017).
12. Yonesaka, K. et al. Autocrine Production of Amphiregulin Predicts Sensitivity to Both Gefitinib and Cetuximab in EGFR Wild-type Cancers. *Clin. Cancer Res.* **14**, 6963–6973 (2008).
13. Jacobs, B. et al. Amphiregulin and Epiregulin mRNA Expression in Primary Tumors Predicts Outcome in Metastatic Colorectal Cancer Treated With Cetuximab. *J. Clin. Oncol.* **27**, 5068–5074 (2009).
14. Stahler, A. et al. Amphiregulin Expression Is a Predictive Biomarker for EGFR Inhibition in Metastatic Colorectal Cancer: Combined Analysis of Three Randomized Trials. *Clin. Cancer Res.* **26**, 6559–6567 (2020).
15. Miranda, O., Farooqui, M. & Siegfried, J. Status of Agents Targeting the HGF/c-Met Axis in Lung Cancer. *Cancers* **10**, 280 (2018).
16. Jeffers, M., Rong, S. & Vande Woude, G. F. Hepatocyte growth factor/scatter factor—Met signaling in tumorigenicity and invasion/metastasis. *J. Mol. Med.* **74**, 505–513 (1996).
17. Khambata-Ford, S. et al. Expression of Epiregulin and Amphiregulin and K-ras Mutation Status Predict Disease Control in Metastatic Colorectal Cancer Patients Treated With Cetuximab. *J. Clin. Oncol.* **25**, 3230–3237 (2007).

18. Lindzen, M. et al. Targeting autocrine amphiregulin robustly and reproducibly inhibits ovarian cancer in a syngeneic model: roles for wildtype p53. *Oncogene* **40**, 3665–3679 (2021).
19. Busser, B., Sancey, L., Brambilla, E., Coll, J.-L. & Hurbin, A. The multiple roles of amphiregulin in human cancer. *Biochimica et. Biophysica Acta (BBA) - Rev. Cancer* **1816**, 119–131 (2011).
20. Singh, S. S. et al. Amphiregulin in cellular physiology, health, and disease: Potential use as a biomarker and therapeutic target. *J. Cell. Physiol.* **237**, 1143–1156 (2022).
21. Jiang, J. et al. Over expression of amphiregulin promoted malignant progression in gastric cancer. *Pathol. - Res. Pract.* **215**, 152576 (2019).
22. Yotsumoto, F. et al. Efficacy of Ligand-based Targeting for the EGF System in Cancer. *Anticancer Res.* **29**, 4879–4885 (2009).
23. Allen, B. M. et al. Systemic dysfunction and plasticity of the immune macroenvironment in cancer models. *Nat. Med.* **26**, 1125–1134 (2020).
24. Bonaventura, P. et al. Cold Tumors: A Therapeutic Challenge for Immunotherapy. *Front. Immunol.* **10**, 168 (2019).
25. Zaiss, D. M. W., Gause, W. C., Osborne, L. C. & Artis, D. Emerging Functions of Amphiregulin in Orchestrating Immunity, Inflammation, and Tissue Repair. *Immunity* **42**, 216–226 (2015).
26. Ko, J. H., Kim, H. J., Jeong, H. J., Lee, H. J. & Oh, J. Y. Mesenchymal Stem and Stromal Cells Harness Macrophage-Derived Amphiregulin to Maintain Tissue Homeostasis. *Cell Rep.* **30**, 3806–3820.e3806 (2020).
27. Dietmar et al. Amphiregulin Enhances Regulatory T Cell-Suppressive Function via the Epidermal Growth Factor Receptor. *Immunity* **38**, 275–284 (2013).
28. Wang, S. et al. Amphiregulin Confers Regulatory T Cell Suppressive Function and Tumor Invasion via the EGFR/GSK-3β/Foxp3 Axis. *J. Biol. Chem.* **291**, 21085–21095 (2016).
29. Minutti, C. M. et al. A Macrophage-Pericyte Axis Directs Tissue Restoration via Amphiregulin-Induced Transforming Growth Factor Beta Activation. *Immunity* **50**, 645–654.e646 (2019).
30. Kaiser, K. A., Loffredo, L. F., Santos-Alexis, K. D. L., Ringham, O. R. & Arpaia, N. Regulation of the alveolar regenerative niche by amphiregulin-producing regulatory T cells. *J. Exp. Med.* **220**, e20221462 (2022).
31. Xu, Q. et al. Targeting amphiregulin (AREG) derived from senescent stromal cells diminishes cancer resistance and averts programmed cell death 1 ligand (PD-L1)-mediated immunosuppression. *Aging Cell* **18**, e13027 (2019).
32. Shields, M. D., Marin-Acevedo, J. A. & Pellini, B. Immunotherapy for Advanced Non–Small Cell Lung Cancer: A Decade of Progress. *American Society Clin. Oncol. Educational Book* **41**, e105-e127 (2021).
33. Seligmann, J. F. et al. Combined Epiregulin and Amphiregulin Expression Levels as a Predictive Biomarker for Panitumumab Therapy Benefit or Lack of Benefit in Patients WithRASWild-Type Advanced Colorectal Cancer. *JAMA Oncol.* **2**, 633 (2016).
34. Yonesaka, K. et al. Combined Analysis of Plasma Amphiregulin and Heregulin Predicts Response to Cetuximab in Metastatic Colorectal Cancer. *PLOS ONE* **10**, e0143132 (2015).
35. Kim, S.-A. et al. Amphiregulin can predict treatment resistance to palliative first-line cetuximab plus FOLFIRI chemotherapy in patients with RAS wild-type metastatic colorectal cancer. *Sci. Rep.* **11**, 23803 (2021).
36. Kim, J.-W. et al. Amphiregulin confers trastuzumab resistance via AKT and ERK activation in HER2-positive breast cancer. *J. Cancer Res. Clin. Oncol.* **142**, 157–165 (2016).
37. Yamada, M. et al. Amphiregulin Is a Promising Prognostic Marker for Liver Metastases of Colorectal Cancer. *Clin. Cancer Res.* **14**, 2351–2356 (2008).
38. Chayangsu, C., Khunsri, S., Sriuranpong, V. & Tanasanvimon, S. The correlations between serum amphiregulin and other clinicopathological factors in colorectal cancer. *J. Gastrointest. Oncol.* **8**, 980–984 (2017).
39. Addison, C. L. et al. Plasma Transforming Growth Factor α and Amphiregulin Protein Levels in NCIC Clinical Trials Group BR.21. *J. Clin. Oncol.* **28**, 5247–5256 (2010).
40. Ishikawa, N. et al. Increases of Amphiregulin and Transforming Growth Factor-α in Serum as Predictors of Poor Response to Gefitinib among Patients with Advanced Non–Small Cell Lung Cancers. *Cancer Res.* **65**, 9176–9184 (2005).
41. Carvalho, S. et al. An antibody to amphiregulin, an abundant growth factor in patients' fluids, inhibits ovarian tumors. *Oncogene* **35**, 438–447 (2016).
42. Su, X. et al. miR-33a-3p regulates METTL3-mediated AREG stability and alters EMT to inhibit pancreatic cancer invasion and metastasis. *Sci. Rep.* **13**, 13587 (2023).
43. Busser, B. et al. Amphiregulin promotes BAX inhibition and resistance to gefitinib in non-small-cell lung cancers. *Mol. Ther.* **18**, 528–535 (2010).
44. Busser, B. et al. Amphiregulin promotes resistance to gefitinib in nonsmall cell lung cancer cells by regulating Ku70 acetylation. *Mol. Ther.* **18**, 536–543 (2010).
45. Dahlhoff, M., Schäfer, M., Wolf, E. & Schneider, M. R. Genetic deletion of the EGFR ligand epigen does not affect mouse embryonic development and tissue homeostasis. *Exp. Cell Res.* **319**, 529–535 (2013).
46. Cerami, E. et al. The cBio cancer genomics portal: an open platform for exploring multidimensional cancer genomics data. *Cancer Discov.* **2**, 401–404 (2012).
47. de Bruijn, I. et al. Analysis and Visualization of Longitudinal Genomic and Clinical Data from the AACR Project GENIE Biopharma Collaborative in cBioPortal. *Cancer Res.* **83**, 3861–3867 (2023).
48. Gao, J. et al. Integrative analysis of complex cancer genomics and clinical profiles using the cBioPortal. *Sci. Signal* **6**, pl1 (2013).
49. R Core Development Team. R: A Language and Environment for Statistical Computing. (R Foundation for Statistical Computing, Vienna, Austria, 2010).

Acknowledgements

We thank Joshua Curtin, Mingxuan Xia, Bharvin Patel, Eilyn Lacy and Fred Kaplan for their helpful discussions. We thank Christopher Moy for the guidance in analyzing the TCGA data. We thank Nicholas Hein and Xuechen Wang for their help in validating and executing statistical tests. We are also indebted to the patients and volunteers who donated the samples used in this study.

Author contributions

R.R.S. was involved in the experimental design, conceptualizing, execution of experiments, analysis and interpretation of data, supervision, and manuscript preparation. B.H. was involved in conceptualizing, experimental designing, analyzing, and interpreting data and manuscript editing. M.P., M.W., K.P.V., S.L.L., and H.G. were involved in the execution of experiments, data analysis, and manuscript editing. S.V. and T.S.Y. were involved in the experimental design, data interpretation, and manuscript editing. SL was involved in interpreting data, resources, and manuscript reviewing and editing. S.M. was involved in the conceptualization, design, supervision, analysis, resources, data interpretation, and manuscript reviewing and editing.

Competing interests

R.R.S., B.H., S.L., H.G., M.W., S.V., T.S.Y. are current employees of Johnson & Johnson but declare no non-financial competing interests. S.L. and S.M. are former employees of Johnson & Johnson but declare no non-financial competing interests. MP and KPV declare no competing interests. S.M. and

B.H. reports a patent application for US17/687,984 - Treatment of Cancers Lacking EGFR- Activating Mutations, pending. S.M reports a patent US9593164B2 - bispecific EGFR/Met antibodies, issued.

Additional information

Supplementary information The online version contains supplementary material available at https://doi.org/10.1038/s41698-024-00682-y.

Correspondence and requests for materials should be addressed to Ricardo Rivera-Soto.